Harmonic Model and Remedy Strategy of Multiphase PM Motor under Open-Circuit Fault

Kok-Meng Lee, *Fellow, IEEE/ASME*, Lei Li, Kun Bai*, *Member, IEEE/ASME*, Xiaoping Ouyang and Huayong Yang

***Abstract*—Modular multiphase (MMP) PM motors have the ability to work continuously under a faulty mode. However, ripples in the spin torque of the motor and unbalanced forces incur rotor vibrations in post-fault operations, which seriously degrade the performance of the PM motors. This paper presents a computationally efficient method to derive harmonic models for characterizing the pulsating torque and unbalanced forces of a MMP-PM motor under an open-circuit fault, and the corresponding optimal solutions to its inverse current model to remedy the fault. The model formulation, current harmonic identification and remedial strategy for suppressing torque ripples and unbalanced forces are illustrated with a MMP-PM motor under an open-circuit fault; both odd and even number of phases are considered. The effectiveness of the harmonic models and remedy strategies are numerically validated with two typical (5- and 6-phase) MMP-PM motors under a one-phase/open-circuit fault, and evaluated experimentally on a custom-designed 6-phase duplex motor**.

***Index Terms*—Harmonics, Inverse Model, Open-circuit, PM motor, Torque ripple, Unbalanced forces.**

NOMENCLATURE

Capitalized symbols

$\mathbf{A}$	Motor system matrix (linearly linking $\mathbf{Q}$ with $\mathbf{x}$).
B_r, B_φ, B_z	(r, φ, Z) components of net MFD
N_C, N_E	Number of (EMs/phase, EMs)
N_f	Number of force/torque harmonic components
N_G, N_k	Number of (groups, current harmonic components)
N_P, N_{ph}	Number of (PM pole-pairs, phases)
$\mathbf{Q}$, $\mathbf{Q}_d$	(Actual, desired) output vector of force f and torque τ
$\mathbf{Q}_g$	The g^{th} component of $\mathbf{Q}$ under the 1P-OC fault.
$\mathbf{Z}$, $\mathbf{Z}_g$	Position-independent coefficient matrix and its g^{th} element

Lowercase symbols

$\mathbf{a}_m$, $\mathbf{a}_c$, $\mathbf{a}_{g\pm}$	Force/torque gain vectors of the (m^{th} phase, c^{th} EM, g^{th} group)
$\mathbf{g}_{g\pm}$	Harmonic vector of the g^{th} group current
$\mathbf{i}$, $\mathbf{i}_g$	Position-independent current vector and its g^{th} element
$\mathbf{q}_r$	Position-independent force/torque reference vector
$\mathbf{x}$	Current vector

Greek symbols

α_{gk}	The k^{th} current harmonic phase angle of the g^{th} group.
β_c, ϕ_m	Position of the c^{th} stator-EM winding and the m^{th} phase
$\mathbf{\Gamma}(\cdot)$	Rotation matrix
$\boldsymbol{\gamma}$	Open-circuit fault indicator matrix
τ_d	Desired ripple-free torque
$\varepsilon_\pm$	Sign indicator of the harmonic interactions
φ, θ	Angular position in XYZ frame and rotor angular position
ζ	Copper loss ratio

This work was supported in part by National Science Foundation of China under Grant U1713204, in part by U. S. National Science Foundation under Grant CMMI-1662700 and in part by National Basic Research Program of China (973 Program) under Grant 2013CB035803.

K.-M. Lee and K. Bai are with the State Key Lab of Digi. Manuf. Equip. and Tech., Huazhong Univ. of Sci. and Tech., Wuhan 430074, China. K.-M. Lee is also Professor of the Woodruff Sch. of Mech. Eng., Georgia Inst. of Tech., Atlanta, GA 30332 USA.

L. Li, X. Ouyang and H. Yang are with the State Key Lab of Fluid Power and Mechatronics Systems, Zhejiang Uni., Hangzhou 310027, China.

**Corresponding author*: kbai@hust.edu.cn.

I. INTRODUCTION

MMP-PM motors are PM motors with modular windings [1~6] designed to achieve electrical, magnetic, thermal and physical isolation among phases. Due to their high power-density, inherent fault-tolerant ability and independent controllability, they have been widely used in a wide variety of applications ranging from more-electric aircraft [2] to [4], metal-removal machining [5] to robotics [6]. Special attentions must be paid to the fault-tolerant design and/or control [2] [7] of the MMP-PM motors so that safety-critical systems driven by these motors will continue working and sustain acceptable performance under various faulty modes. The most probable fault is the loss of 1-phase due to an open-circuit fault [8]. The open-circuit fault of a phase can be easily detected by monitoring the load currents [9]. However, large spin-torque ripples (or variations about the average spin-torque) and unbalanced magnetic forces acting on the rotor exist in the post-fault operations, which incur serious vibrations and degraded performance of the PM motors. To sustain acceptable post-fault performance, a method to identify the current harmonic components for compensating the pulsating torque and unbalanced forces, and compute the corresponding optimal currents in real-time to remedy its open-circuit fault is required.

MMP-PM motors are custom-designed [10] [11] to eliminate unbalanced radial forces under healthy modes, which often take advantages of the diametrically symmetrical electromagnetic (EM) windings; for examples, [2] to [5]. A 6-phase PM motor as a dual 3-phase PM motor was designed in [4] [12] to simplify the control algorithm under a faulty mode. However, the loss of any phase will lead to diametrically asymmetrical windings [13] and/or asymmetrical input currents [10] [11] resulting in reduced average torque with large ripples and unbalanced radial forces [4] [8], even if a PM motor was initially designed for low torque ripple and balanced radial forces.

Under a healthy mode, torque ripples (caused by the interactions between the harmonics of the back electromotive force and that of the input currents) can be compensated using the solutions to a harmonic model as demonstrated in [14], which can be extended to torque control of a MMP-PM motor under faulty modes. Considering only the harmonics of the fundamental and third currents, Bianchi *et.al* [15][16] analytically derived the currents minimizing the torque-ripple for post-fault operations of a modular 5-phase motor although the average torque decreases under faulty modes. Parsa *et.al* [17] proposed a unified fault-tolerant current-control approach to increase the average output torque while minimizing torque ripples and copper losses for a 5-phase PM motor under various faulty modes. Similar works considering only the fundamental current component to develop a specified torque were also reported in [8]. Based on the reduced-order Park-Clark transformation, the optimal currents remedying the open-circuit

fault was derived in the field-orientated control scheme utilizing fundamental current [18][19] or 3rd harmonic current injection method [20]. Different from the harmonic-based methods, Wang *et.al* [10] [11] [21] designed a time-domain optimal torque controller under voltage constraints for a modular 5-phase PM motor to ensure a ripple-free torque output with minimum copper loss under healthy and faulty modes. It is found that the derived optimal currents are dominated by the fundamental and 3rd harmonic with a small 5th harmonic component [21].

Previous research efforts on torque control of MMP-PM motors generally do not consider suppressing the unbalanced forces under an open-circuit fault, although mentioned in [12] [22]. To sustain the torque output capacity, the currents of the remaining healthy phases need to be properly amplified, which may lead to larger unbalanced forces in post-fault operations. Due to the lack of computationally efficient harmonic models, the harmonic components accounted for in the remedy currents are limited to the fundamental and 3rd components in existing techniques [8, 15-20]. While in the time-domain methods [21], the harmonics orders of the derived currents cannot be pre-determined [23]. To overcome the above challenges, this paper presents a computationally efficient method to derive harmonic models and their inverse solutions for analyzing and suppressing torque ripples and unbalanced forces of a MMP-PM motor under an open-circuit fault; for clarity in illustration, a 1-phase open-circuit (1P-OC) fault is used as an example. The remainder of this paper offers the following:

- Section II begins with the force/torque equation of a MMP-PM motor and its time-based inverse solutions. To overcome their limitations, a model that characterizes the harmonic components of pulsating torque and unbalanced forces of a motor is derived to identify the required current harmonics and compute an optimal set of currents in real-time to ensure a ripple-free torque. As will be analytically illustrated, the harmonic method leads to a unified inverse model for suppressing torque ripples and unbalanced forces in a MMP-PM motor under a 1P-OC-fault, while allowing for different remedy strategies characterized by an odd or even number of phases.
- In Section III, the harmonic models are numerically illustrated and validated with two typical (5- and 6-phase) motors. The effectiveness of the fault remedial strategy for suppressing torque ripples and unbalanced radial forces has been evaluated experimentally on a custom-designed 6-phase PM motor operated under a 1P-OC fault.

II. Fault Remedy of MMP-PM Motors

Consider a single-axis MMP-PM motor with N_P PM pole-pairs (surface-mounted on the rotor) and N_E stator EMs. Figures 1(a, b) show two common PM-motor design structures, axial-flux and radial-flux [5], where *XYZ* and *xyz* are the stator (reference) and rotor (moving) coordinate frames respectively; and *Z* and *z* are on a common axis about which the rotor displacement θ is measured from the *X*-axis. In the event of open-circuit fault, the unbalanced forces (along the *X*- and *Y*-axes) and large ripples in the reduced average torque would seriously degrade the MMP-PM motor performance. To sustain an acceptable performance of the motor during the post-fault operations, an inverse model is incorporated in the speed control system as shown in Fig. 1(c) to compute the remedy currents required to generate the specified torque τ_d while eliminating the unbalanced forces (f_x, f_y). As will be shown, the computation of the remedy currents for real-time implementation is divided into two parts as illustrated in Fig. 1(d); a position-independent inverse model which can be calculated offline, and a harmonic-based kernel vector which updates the desired remedy currents in real-time.

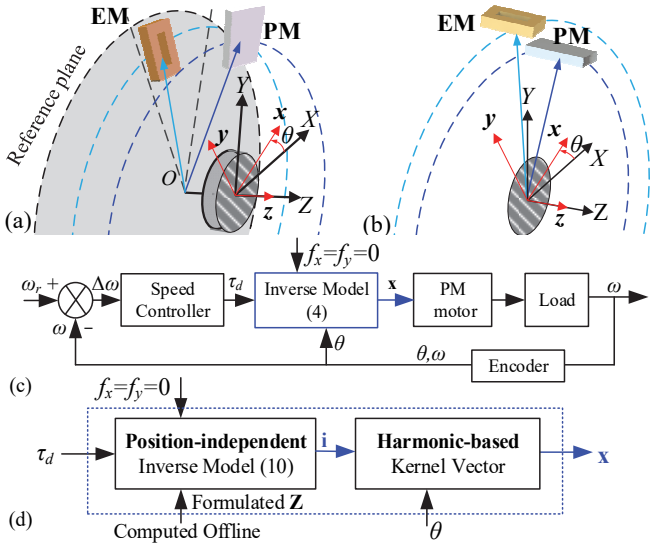

Fig. 1 MMP-PM motor and speed-control system for 1P-OC fault remedy. (a) Axial-flux type. (b) Radial-flux type. (c) Time-based Inverse Model. (d) Harmonic-based remedy strategy.

The following assumptions are made in the derivation:

1) The spatially distributed PM remanences are symmetric about its center.
2) The $N_E = N_C N_{ph}$ stator EM-windings are evenly grouped into N_{ph} phases; each with N_C EM windings.
3) The eddy-currents and end-fringing have negligible effects on the magnetic field in the stator/rotor air-gap.

To ensure safe operation in the event of an open-circuit fault, the PM motor is designed such that its input current vector **x** (with element i_m where m=1, 2… N_{ph}) has a higher dimension than its output force/torque vector **Q**, where **Q** and **x** are defined in terms of the rotor position θ:

$$\mathbf{x}(\theta) = \left[i_1(\theta) \cdots \quad i_m(\theta) \quad \cdots i_{N_{ph}}(\theta) \right]^{\mathrm{T}} \tag{1a}$$

$$\mathbf{Q}(\theta) = \left[f_x(\theta) \quad f_y(\theta) \quad \tau(\theta) \right]^{\mathrm{T}} \tag{1b}$$

The unbalanced forces (f_x, f_y) and pulsating torque $\tau(\theta)$ are described in the (forward) torque model (2a) that determines **Q** in terms of **x** for analyzing and controlling a PM motor:

$$\mathbf{Q}(\theta) = \left[\mathbf{A}(\theta)\boldsymbol{\gamma} \right] \mathbf{x} + \left(\mathbf{K}\boldsymbol{\gamma} \right) \mathbf{x}.^2 + \mathbf{Q}_P(\theta) \tag{2a}$$

$$\text{where } \mathbf{A}\left(\mathbb{R}^{3\times N_{ph}} \right) = \left[\mathbf{a}_1(\theta) \quad \ldots \quad \mathbf{a}_m(\theta) \quad \ldots \quad \mathbf{a}_{N_{ph}}(\theta) \right] \tag{2b}$$

$$\text{and } \mathbf{K}\left(\in \mathbb{R}^{3\times N_{ph}} \right) = \left[\mathbf{k}_1 \quad \ldots \quad \mathbf{k}_m \quad \ldots \quad \mathbf{k}_{N_{ph}} \right]. \tag{2c}$$

In (2a), $\mathbf{x}.^2 = \left[i_1^2 \ldots i_m^2 \ldots \right]^{\mathrm{T}}$. Formulated in terms of the rotor position θ, (2a) is referred to here as the time-based forward model of the MMP-PM motor. For a specified θ, the 1st term (linear with **x**) in **Q** is contributed by the Lorentz force between

the current-carrying conductors and PMs; the 2nd term (quadratic with **x**) and $\mathbf{Q}_P$ correspond to the forces/torque between the (EMs, PMs) and the iron-cores respectively. In (2a), the diagonal matrix $\boldsymbol{\gamma}$ (with binary elements γ_m where m=1…N_{ph}) acts as a fault indicator to account for different operating modes. The element γ_m normally takes the value of 1; a value of 0 indicates that the m^{th} phase is physically open-circuit or fail. Thus, $\boldsymbol{\gamma}$ does not depend on rotor displacement, and $\mathbf{A}(\theta)$ is independent of the operating mode. In (2b), the vector $\mathbf{a}_m$ depends on the layout of N_C stator-EM windings in the m^{th} phase, and can be derived from the vector $\mathbf{a}_c$=[a_{xc} a_{yc} $a_{\tau c}$]$^{\text{T}}$ for the c^{th} stator-EM winding at angular position β_c where (a_{xc}, a_{yc}) are the force/current gains along (X, Y) axes and $a_{\tau c}$ is the torque/current gain:

$$\mathbf{a}_m(\theta,\ \phi_m) = \sum \mathbf{a}_c(\theta,\ \beta_c) \tag{3a}$$

$$\text{where } \phi_m = \phi_1 + \frac{2\pi(m-1)}{N_{ph}} \text{ and } \beta_c = \beta_1 + \frac{2\pi(c-1)}{N_E} \tag{3b,c}$$

In (3b, c), ϕ_1 and β_1 are the angular positions of the 1st phase and stator-EM respectively; and ϕ_m is the m^{th} phase position.

In (2c), $\mathbf{k}_m \in \mathbb{R}^{3\times 1}$ (m=1 … N_{ph}) is the m^{th} column vector of **K**. For iron surface-mounted MMP-PM motors (non-salient rotor and even slot number), **K** that contributes only force (and no torque) production is negligibly small due to the relatively large effective air-gap height [22], while $\mathbf{Q}_P$ has only the torque component [13] (cogging torque) that can be reduced by design techniques. For an ironless PM motor, **K**=$\mathbf{Q}_P$=**0** and **Q**=**A**(θ)**x** can be computed directly using the Lorentz force equation [5] [24]. Hence, **K** and $\mathbf{Q}_P$ are ignored in the inverse model.

In the event of an open-circuit fault, it is highly desired that **Q** behaves like $\mathbf{Q}_d$=[0, 0, τ_d]$^{\text{T}}$ (or f_x=f_y=0) where the ripple-free (position-independent) torque τ_d is calculated by a speed controller to compensate for the error $\Delta\omega$ between the reference speed ω_r and measured speed ω as shown in Fig. 1(c). In the case of torque control, τ_d is directly specified as a torque reference. For a current-controlled ironless motor with more number of active current phases than the dimension of $\mathbf{Q}_d$, an optimal **x** that minimizes the copper loss and satisfies $\mathbf{Q}_d$ can be directly computed from the pseudo-inverse of matrix **A**(θ) [5]:

$$\mathbf{x}(\theta) = \boldsymbol{\gamma}^{\text{T}}\mathbf{A}^{\text{T}}(\theta)\left[\mathbf{A}(\theta)\boldsymbol{\gamma}\boldsymbol{\gamma}^{\text{T}}\mathbf{A}^{\text{T}}(\theta)\right]^{-1}\mathbf{Q}_d \tag{4}$$

where $\boldsymbol{\gamma}$ is incorporated into (4) to account for the open-circuit fault. Equation (4) is referred to here as the time-based inverse model of the MMP-PM motor. However, the optimal **x** derived from (4) depends on the rotor displacement θ, and the matrix inversion involved in (4) must determine **A**(θ) from a pre-computed look-up table of single input and multiple outputs, which is computationally inefficient as it generally requires a relatively large memory and time [23] especially for a MMP-PM motor with large N_{ph}.

A. Harmonic-based Fault Remedy

For a specified position-independent $\mathbf{Q}_d$ and $\boldsymbol{\gamma}$ that acts as a fault indicator in the first term of (2a), **x**(θ) derived from (4) only depends on **A**(θ) that is independent of the operating mode and repeats as the rotor spins $2\pi/N_P$. Hence, (**A**, **x**) are periodic (period $2\pi/N_P$) and can be formulated in harmonic forms [25] even in the event of open-circuit fault. As derived in Appendix for both axial- and radial-flux MMP-PM motors, $\mathbf{a}_c$ in (3) can be described in terms of (radial, tangential) force/current gains (a_{rc}, $a_{\varphi c}$) and $a_{\tau c}$, which are expressed in harmonic forms in (5b) with (a_{rj}, $a_{\varphi j}$, $a_{\tau j}$) being the j^{th} harmonic amplitudes of (a_{rc}, $a_{\varphi c}$, $a_{\tau c}$) respectively:

$$\mathbf{a}_c(\beta_c,\theta) = \begin{bmatrix} a_{xc} \\ a_{yc} \\ a_{\tau c} \end{bmatrix} = \begin{bmatrix} \boldsymbol{\Gamma}(\beta_c) & \mathbf{0}_{2\times 1} \\ \mathbf{0}_{1\times 2} & 1 \end{bmatrix} \begin{bmatrix} a_{rc} \\ a_{\varphi c} \\ a_{\tau c} \end{bmatrix} \tag{5a}$$

$$\text{where } \begin{bmatrix} a_{rc} \\ a_{\varphi c} \\ a_{\tau c} \end{bmatrix} = \sum_{j=1,3,5\ldots}^{\infty} \begin{bmatrix} a_{rj}\cos jN_p(\theta-\beta_c) \\ a_{\varphi j}\sin jN_p(\theta-\beta_c) \\ a_{\tau j}\sin jN_p(\theta-\beta_c) \end{bmatrix} \tag{5b}$$

$$\text{and } \boldsymbol{\Gamma}(\bullet) = \begin{bmatrix} \cos(\bullet) & -\sin(\bullet) \\ \sin(\bullet) & \cos(\bullet) \end{bmatrix}. \tag{5c}$$

Equations (3) and (5) provide a basis to identify the harmonic components (j=1, 3, 5 …) of the force/torque vector in (2b).

A.1 Phase regrouped under a 1P-OC fault

In the event of a 1P-OC fault, the operating healthy phases are reorganized into N_G strategic groups for fault remedy, which depends on the odd or even number of phases, N_{ph}. As illustrated in Fig. 2(a, b) where Phase 1 at ϕ_1 is assumed to have an open-circuit fault, a new Cartesian system OX_1Y_1 with its X_1-axis aligned with the open-circuit phase is assigned:

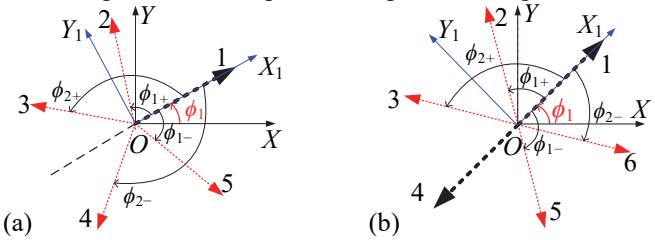

Fig. 2 MMP-PM motors with odd and even N_{ph}. (a) N_{ph}=5, (b) N_{ph}=6.

For odd N_{ph}, the (N_{ph}−1) healthy phases are regrouped into N_G=(N_{ph}−1)/2 symmetrical groups about the X_1-axis. As an example, the 5-phase motor (Fig. 2a) will have N_G=2 groups; Phases (2, 5) at $\phi_{1\pm}$ and Phases (3, 4) at $\phi_{2\pm}$ correspond to g=1 and g=2 groups respectively. The N_G groups can be characterized by their angular positions, $\phi_{g\pm}$=±2πg/N_{ph}.

For even N_{ph}, (N_{ph}−2) of the healthy phases are regrouped into N_G=(N_{ph}−2)/2 groups characterized by their angular positions, $\phi_{g\pm}$=2πg/N_{ph}−π/2(1 ∓ 1), so that the advantage of the diametrical symmetry can be kept. As illustrated in Fig. 2(b), the 6-phase motor will have N_G=2 groups; Phases (2, 5) at $\phi_{1\pm}$ and Phases (3, 6) at $\phi_{2\pm}$ correspond to g=1 and g=2 groups respectively. In this scheme, Phase 4 is sacrificed so that no additional current is needed to compensate unbalanced forces [5] caused by the loss of symmetry due to the failed Phase 1.

A.2 Inverse model for a 1P-OC fault remedy

Under the 1P-OC fault, the current flowing through the g^{th} group (where g=1, 2… N_G) at ϕ_{g+} or ϕ_{g-} is denoted as i_{g+} or i_{g-} respectively. The regrouped current $i_{g\pm}(\theta)$, which characterizes the identified current harmonics, is decoupled into a position-independent column vector $\mathbf{i}_g$ and a position-dependent kernel vector $\mathbf{g}_{g\pm}(\theta)$ that depends on odd or even N_{ph} to be discussed in Sections *II.B* and *II.C*. For practical implementation, finite N_k harmonic components of the $i_{g\pm}(\theta)$ in the N_G groups are considered. Consequently, a position-independent vector **i** accounting for all the currents in the N_G groups and hence **x**(θ)

in (2a) can be described as (6a~d) where $\mathbf{i}_{gk}$ corresponds to the k^{th} current harmonics of the g^{th} group current $\mathbf{i}_g$:

$$\mathbf{i}^{\mathrm{T}} = \begin{bmatrix} \mathbf{i}_1^{\mathrm{T}} \cdots & \mathbf{i}_g^{\mathrm{T}} & \cdots \mathbf{i}_{N_G}^{\mathrm{T}} \end{bmatrix} \tag{6a}$$

$$i_{g\pm}(\theta) = \mathbf{g}_{g\pm}(\theta)\mathbf{i}_g \text{ where } \mathbf{i}_g^{\mathrm{T}} = [\ldots \quad \mathbf{i}_{gk}^{\mathrm{T}} \quad \ldots]. \tag{6b,c}$$

$$\mathbf{x}^{\mathrm{T}} = \begin{cases} \begin{bmatrix} 0 & i_{1+}\cdots & i_{g+}\cdots & \cdots i_{g-} & \cdots i_{1-} \end{bmatrix} & \text{Odd } N_{ph} \\ \begin{bmatrix} 0 & i_{1+}\cdots & i_{g+}\cdots & i_{1-}\cdots & i_{g-}\cdots \end{bmatrix} & \text{Even } N_{ph} \end{cases} \tag{6d}$$

The force/torque vector $\mathbf{Q}$ in (2a) is essentially the sum of the ($g = 1 \ldots N_G$) individual force/torque vectors $\mathbf{Q}_g$, and consists of a steady-state component $\bar{\mathbf{Q}}$ and N_f ripple harmonics $\hat{\mathbf{Q}}_n$:

$$\mathbf{Q}(\theta) = \sum_{g=1}^{N_G} \mathbf{Q}_g(\theta) = \bar{\mathbf{Q}} + \sum_{n=1}^{N_f} \hat{\mathbf{Q}}_n(\theta) \tag{7a}$$

$$\text{where } \mathbf{Q}_g(\theta) = \mathbf{a}_{g_+}(\theta)\mathbf{g}_{g_+}(\theta)\mathbf{i}_g + \mathbf{a}_{g_-}(\theta)\mathbf{g}_{g_-}(\theta)\mathbf{i}_g \tag{7b}$$

$$\text{and} \quad \mathbf{a}_{g\pm}(\theta) = \begin{bmatrix} a_{xg\pm} & a_{yg\pm} & a_{\tau g\pm} \end{bmatrix}^{\mathrm{T}} \tag{7c}$$

In (7c), ($a_{xg\pm}$, $a_{yg\pm}$) are the force/current gains along the (X, Y) axes, and $a_{\tau g\pm}$ is the torque/current gain of the g^{th} group. Mathematically, the objectives are

$$\bar{\mathbf{Q}} = \mathbf{Q}_d = \begin{bmatrix} 0 & 0 & \tau_d \end{bmatrix}^{\mathrm{T}} \text{ and } \hat{\mathbf{Q}}_n = \mathbf{0}_{3\times 1} \tag{7d,e}$$

By arranging the $\bar{\mathbf{Q}}(= \mathbf{Q}_d)$ and $\hat{\mathbf{Q}}_n$ in the increasing order of the harmonics, (7d, e) can be compactly expressed as a position-independent reference (column) vector $\mathbf{q}_r$:

$$\mathbf{q}_r \in \mathbb{R}^{3(1+N_f)\times 1} = \begin{bmatrix} \mathbf{Q}_d^{\mathrm{T}} & \mathbf{0} & \cdots & \mathbf{0} \end{bmatrix}^{\mathrm{T}} \tag{8}$$

With (6a), (7a,b) and (8), an alternative position-independent forward model is formulated in (9a, b) where the submatrix $\mathbf{Z}_g$ in the coefficient matrix $\mathbf{Z}$ is contributed by the g^{th} group:

$$\mathbf{Z}\mathbf{i} = \mathbf{q}_r \text{ where } \mathbf{Z} = \begin{bmatrix} \mathbf{Z}_1 \ldots & \mathbf{Z}_g & \ldots \mathbf{Z}_{N_G} \end{bmatrix} \tag{9a,b}$$

By comparing the given $\mathbf{a}_{g\pm}(\theta)\mathbf{g}_{g\pm}(\theta)$ terms in (7b) with the position-independent sub-matrix $\mathbf{Z}_g$ of (9a, b), the harmonic components of $\mathbf{Q}_g$ can be identified for formulating $\mathbf{Z}_g$. The corresponding position-independent pseudo-inverse model that derives an optimal $\mathbf{i}$ minimizing the copper loss [14] for a reference vector $\mathbf{q}_r$ in a MMP-PM motor under the 1P-OC fault (Fig. 1d) is given by

$$\mathbf{i} = \mathbf{Z}^{\mathrm{T}} \left[\mathbf{Z}\mathbf{Z}^{\mathrm{T}} \right]^{-1} \mathbf{q}_r \tag{10}$$

As shown in Fig. 1(d), the inverse harmonic model consists of (6a~d) and (10) where the position-independent $\mathbf{Z}$ can be computed offline for an optimal $\mathbf{i}$ for updating the optimal $\mathbf{x}$ that requires a simple multiplication once the harmonic-based kernel vector (6b) is available. Thus, the optimal currents can be calculated in real-time to remedy the 1P-OC fault, which eliminate the unbalanced forces (f_x, f_y) and generate a desired ripple-free torque τ_d. The proposed inverse harmonic model for fault remedy in Fig. 1(d) accomplishes the tasks undertaken by the time-based inverse model (4) while overcoming its limitations. Depending on odd or even N_{ph}, the relationships between $\mathbf{a}_{g+}(\theta)$ and $\mathbf{a}_{g-}(\theta)$, and that $\mathbf{g}_{g+}(\theta)$ and $\mathbf{g}_{g-}(\theta)$ may differ. For clarity, the 1P-OC remedy strategy for a MMP-PM motor with an odd N_{ph} and that with an even N_{ph} are separately formulated in Sections II.B and II.C respectively.

B. Odd-phase Remedy Strategy (ORS)

Without loss of generality, we assume N_E=N_{ph} and β_c=ϕ_m with c=m=1… N_{ph} for clarity in illustrating the formulation of a remedy strategy for MMP-PM motors with an odd N_{ph} [10] [11], in other words, each phase consists of one stator-EM winding and unbalanced forces result in the event of the 1P-OC fault. Based on the assumptions above, the following discussions can also account for the simple cases where pairs of diametrically symmetric EM windings are grouped into one phase and there is no need to consider the unbalanced forces. Under the 1P-OC fault, the corresponding relationship between $\mathbf{a}_{g+}$ and $\mathbf{a}_{g-}$ of the g^{th} group can be derived from (5a) in the $\mathrm{OX_1Y_1}$ frame:

$$\begin{bmatrix} a_{xg+}(\phi_{g+}, \theta) \\ a_{yg+}(\phi_{g+}, \theta) \\ a_{\tau g+}(\phi_{g+}, \theta) \end{bmatrix} = \begin{bmatrix} a_{xg-}(\phi_{g-}, -\theta) \\ -a_{yg-}(\phi_{g-}, -\theta) \\ -a_{\tau g-}(\phi_{g-}, -\theta) \end{bmatrix} \tag{11}$$

The last row in (11) suggests that the currents $i_{g\pm}$ should take the form (12) such that $i_{g+}(\phi_{g+}, \theta) = -i_{g-}(\phi_{g-}, -\theta)$ to recover the original torque under the 1P-OC fault:

$$i_{g\pm} = \sum_{k=1,3\ldots}^{N_k} i_{gk} \sin\left(kN_P\theta_{g\pm} \mp \alpha_{gk} \right) \text{ where } \theta_{g\pm} = \theta - \phi_{g\pm} \tag{12}$$

As in (6b, c), (12) where (i_{gk}, α_{gk}) are the k^{th} current harmonic (amplitude, angle from $\theta_{g\pm}$) of the g^{th} group is rewritten in the OXY frame:

$$\mathbf{i}_{gk}^{\mathrm{T}} = i_{gk}\mathbf{h}'(\alpha_{gk}) \tag{13a}$$

$$\mathbf{g}_{g\pm}(\in \mathbb{R}^{1\times 2N_k}) = \begin{bmatrix} \cdots & \mp\mathbf{h}\left(\mp kN_P\left(\theta_{g\pm} - \phi_1 \right) \right) & \cdots \end{bmatrix} \tag{13b}$$

$$\mathbf{h}(\bullet) = \begin{bmatrix} S_{(\bullet)} & C_{(\bullet)} \end{bmatrix} \text{ and } \mathbf{h}'(\bullet) = \begin{bmatrix} C_{(\bullet)} & S_{(\bullet)} \end{bmatrix} \tag{13c,d}$$

In (13c~d), $C_{(\bullet)}$ and $S_{(\bullet)}$ denote the cosine and sine of the angle ($\bullet$) respectively for simplicity in the following discussions.

With (12) along with the force/torque-current gains (5a~c), the resulting $\mathbf{Q}_g$=[f_{xg}, f_{yg}, τ_g]$^{\mathrm{T}}$ in (7b) for the ORS is given by

$$\mathbf{Q}_g = \sum_{j,k=1,3\ldots}^{\infty} \begin{bmatrix} \mathbf{H}_{g(j-k)} & \mathbf{H}_{g(j+k)} \end{bmatrix} \begin{bmatrix} \mathbf{Z}_{g(j-k)} \\ \mathbf{Z}_{g(j+k)} \end{bmatrix} \mathbf{i}_{gk} \tag{14a}$$

$$\text{where } \mathbf{H}_{g(j\pm k)} = diag\begin{pmatrix} S_{\theta_\pm} & C_{\theta_\pm} & C_{\theta_\pm} \end{pmatrix}; \tag{14b}$$

$$\theta_\pm = (j \pm k) N_P \theta; \tag{14c}$$

$$\mathbf{Z}_{g(j\pm k)}(\phi_{g+}) = \begin{bmatrix} \pm\varepsilon_\pm a_{rj} C_{\phi_{g+}} C_{\phi_\pm} \pm \varepsilon_\pm a_{\varphi j} S_{\phi_{g+}} S_{\phi_\pm} & \varepsilon_\pm a_{\varphi j} S_{\phi_{g+}} C_{\phi_\pm} - \varepsilon_\pm a_{rj} C_{\phi_{g+}} S_{\phi_\pm} \\ \mp a_{rj} S_{\phi_{g+}} S_{\phi_\pm} \mp a_{\varphi j} C_{\phi_{g+}} C_{\phi_\pm} & a_{\varphi j} C_{\phi_{g+}} S_{\phi_\pm} - a_{rj} S_{\phi_{g+}} C_{\phi_\pm} \\ \mp a_{\tau j} C_{\phi_\pm} & a_{\tau j} S_{\phi_\pm} \end{bmatrix} \tag{14d}$$

$$\phi_\pm = (j \pm k) N_P \phi_{g+} \text{ and } \varepsilon_\pm = \mathrm{sgn}(j \pm k). \tag{14e,f}$$

In (14a), $\mathbf{H}_{g(j\pm k)}(\theta)$ accounts for the ($j \pm k$)$^{\text{th}}$ harmonic components of the Lorentz force due to the interactions between $\mathbf{a}_{g\pm}(\theta)$ and $i_{g\pm}(\theta)$ for a given N_P. The coefficient matrix $\mathbf{Z}_{g(j\pm k)}$ depends on ($a_{\varphi j}$, a_{rj}, $a_{\tau j}$, $\varepsilon_\pm$, $\phi_\pm$) where $\varepsilon_\pm$ in (14f) is used to negate θ_- when j<k.

Noting that f_{xg} vanishes in the steady-state component $\mathbf{Q}_g$=[0, f_{yg}, τ_g]$^{\mathrm{T}}$ for j=k ($S_{\theta-}$=0) which can be derived from (14a,b); and $\bar{\mathbf{Q}}^{\mathrm{T}}$ reduces to [f_y, τ_d]$^{\mathrm{T}}$. Based on (14c~f), the corresponding $\mathbf{q}_r$ in (8) and $\mathbf{Z}_g$ in (9b) for the ORS can be expressed as (15a~c) where $\mathbf{z}_{g(k\text{-}k)}$ can be derived from (14d) for j=k ($S_{\theta_-} = S_{\phi_-} = 0$, $C_{\theta_-} = C_{\phi_-} = 1$ and ε_-=0):

$$\mathbf{q}_r^{\mathrm{T}}\left(\in \mathbb{R}^{1\times(2+3N_f)} \right) = \begin{bmatrix} 0 & \tau_d & \mathbf{0}_{1\times 3} & \ldots \end{bmatrix} \tag{15a}$$

$$\mathbf{Z}_g\left(\in \mathbb{R}^{(2+3N_f)\times 2N_k}\right)=\begin{bmatrix} \mathbf{z}_{g(1-1)}\cdots & \mathbf{z}_{g(k-k)} & \cdots \\ \vdots\cdots & \vdots & \cdots\vdots \\ \sum_{(j\pm1)=2}\mathbf{Z}_{g(j\pm1)}\cdots & \sum_{|j\pm k|=\hbar}\mathbf{Z}_{g(j\pm k)} & \cdots \\ \vdots\cdots & \vdots & \cdots\vdots \end{bmatrix} \quad (15b)$$

$$\text{and } \mathbf{z}_{g(k-k)}\left(\phi_{g+}\right)=\begin{bmatrix} a_{\varphi j}C_{\phi_{g+}} & -a_{rj}S_{\phi_{g+}} \\ a_{\tau j} & 0 \end{bmatrix} \text{when } j=k \quad (15c)$$

In (15b) that defines the forces/torque contributed by the g^{th} group for the given position-independent $\mathbf{i}_g$, $\hbar$ ($|j\pm k|$ =2, 4,...) indicates the force/torque harmonics order to be eliminated.

C. Even-phase Remedy Strategy (ERS)

For an even N_{ph} motor [4][8], the diametrically symmetric (c, $c\pm N_E/2$) EM-windings belong to the (m, $m\pm N_{ph}/2$) phases respectively. From (5a), $\mathbf{a}_{g+}$ and $\mathbf{a}_{g-}$ are related by

$$\begin{bmatrix} a_{xg+}\left(\theta_{g+}\right) \\ a_{yg+}\left(\theta_{g+}\right) \\ a_{\tau g+}\left(\theta_{g+}\right) \end{bmatrix}=(-1)^{N_P}\begin{bmatrix} -a_{xg-}\left(\theta_{g-}\right) \\ -a_{yg-}\left(\theta_{g-}\right) \\ a_{\tau g-}\left(\theta_{g-}\right) \end{bmatrix} \quad (16)$$

The corresponding currents $i_{g\pm}$ and $\mathbf{g}_{g\pm}(\theta)$ are given in (17a, b) with $\mathbf{i}_{gk}$ defined in (13a):

$$i_{g\pm}=\sum_{k=1,3\ldots}^{N_k} i_{gk}\sin\left(kN_P\theta_{g\pm}-\alpha_{gk}\right) \quad (17a)$$

$$\mathbf{g}_{g\pm}=\begin{bmatrix}\cdots & -\mathbf{h}\left(-kN_P\left(\theta_{g\pm}-\phi_1\right)\right) & \cdots\end{bmatrix} \quad (17b)$$

Different from the forces (f_{xg}, f_{yg}) produced by the g^{th} group consisting of 'mirror-symmetric' phases in Fig. 2(a), (f_{xg}, f_{yg}) are self-balanced (and vanished) for the given currents (17a) due to the diametrically symmetric phases in Fig. 2(b). Hence, the corresponding $\mathbf{Q}_g$ for the case of even N_{ph} reduces to [0, 0, τ_g]$^{\text{T}}$; and the torque τ_g contributed by all the stator-EMs in the g^{th} group can be calculated from (17a) and (5):

$$\tau_g=\sum_{j,k=1,3\ldots}^{\infty}\begin{bmatrix}\mathbf{h}'\left(\theta_-\right) & \mathbf{h}'\left(\theta_+\right)\end{bmatrix}\begin{bmatrix}\mathbf{Z}_{g(j-k)} \\ \mathbf{Z}_{g(j+k)}\end{bmatrix}\mathbf{i}_{gk} \quad (18a)$$

$$\mathbf{Z}_{g(j\pm k)}=N_m a_{\tau j}\begin{bmatrix}\mp C_{\phi_\pm} & S_{\phi_\pm} \\ \mp\varepsilon_\pm S_{\phi_\pm} & -\varepsilon_\pm C_{\phi_\pm}\end{bmatrix} \quad (18b)$$

where ($\theta_\pm$, $\phi_\pm$, $\varepsilon_\pm$) are defined as in (14c, e, f), N_m is the effective number of the EM windings per phase (that contribute the torque production) and determined from (3a). Similar to $\mathbf{H}_{g(j\pm k)}$ in (14b), $\mathbf{h}'(\theta_\pm)$ in (18a) indicates the $(j\pm k)^{\text{th}}$ torque harmonic components due to the interactions of $a_{\tau g\pm}(\theta)$ and $i_{g\pm}(\theta)$. The matrix $\mathbf{Z}_{g(j\pm k)}$ (18b) depends only on ($a_{\tau j}$, $\varepsilon_\pm$, $\phi_\pm$).

When j=k ($S_{\theta-}$=0, $C_{\theta-}$=1), a ripple-free component of [0, 0, τ_g]$^{\text{T}}$ can be obtained in (18a); thus, the corresponding $\mathbf{q}_r$ and $\mathbf{Z}$ for the ERS can be derived from (18) where $\mathbf{q}_r$ is given by (19a) and $\mathbf{Z}_g$ takes the form in (15b) with $\mathbf{z}_{g(k-k)}$ defined in (19b):

$$\mathbf{q}_r^{\text{T}}\in\mathbb{R}^{1\times(1+2N_f)}=\begin{bmatrix}\tau_d & \mathbf{0}_{1\times2} & \ldots & \mathbf{0}_{1\times2}\end{bmatrix} \quad (19a)$$

$$\mathbf{z}_{g(k-k)}\left(\phi_{g+}\right)=\begin{bmatrix}a_{\tau j} & 0\end{bmatrix} \text{ with } j=k \quad (19b)$$

D. Formulation and Computation Procedure

Given a MMP-PM motor with known (N_{ph}, N_C, N_P, N_E) and specified stator-EM winding layout characterized by β_c (where c=1… N_E), the (a_{rj}, $a_{\varphi j}$, $a_{\tau j}$) values (5b) along with the angular position ϕ_1 (3b) that provide a basis for the inverse model formulation can be obtained from $\mathbf{a}_c$ in (5a). The vector $\mathbf{a}_c$ can be expressed in terms of $\mathbf{Q}_P$ and $\mathbf{k}_c$, (20a), where $\mathbf{k}_c$ indicates the forces (along X- and Y-axes) and torque due to the interaction between the c^{th} stator-EM and the rotor iron-core. It can be numerically (A.1) or experimentally obtained by exciting only the c^{th} EM-windings with a constant current I:

$$\mathbf{a}_c=\left(\mathbf{Q}-\mathbf{Q}_P-\mathbf{k}_c I^2\right)/I \quad (20a)$$

To account for the iron effects, $\mathbf{Q}_P(\theta)$ and $\mathbf{k}_c$ are described in (20b) and (20c) respectively. In (20b), the cogging torque $\tau_P(\theta)$ is computed with all the phase open-circuit:

$$\mathbf{Q}_P=\begin{bmatrix}0 & 0 & \tau_P\left(\theta\right)\end{bmatrix}^{\text{T}} \quad (20b)$$

The forces contributed by $\mathbf{k}_c$ point along the Z-axis and radial direction for axial-flux and radial-flux MMP-PM motors respectively, and hence $\mathbf{k}_c$ is characterized in (20c) where the constant K_o is calculated from the armature reaction field:

$$\mathbf{k}_c=\begin{cases}\mathbf{0}_{3\times1} & \text{axial-flux} \\ K_o\begin{bmatrix}C_{\beta_c} & S_{\beta_c} & 0\end{bmatrix}^{\text{T}} & \text{radial-flux}\end{cases} \quad (20c)$$

With the values of $\mathbf{a}_c$ obtained from (20a) at different θ, the components (a_{rc}, $a_{\varphi c}$, $a_{\tau c}$) can be computed with inverse of (5a); and the coefficients (a_{rj}, $a_{\varphi j}$, $a_{\tau j}$) in (5b) can be found by curve-fitting the values of (a_{rc}, $a_{\varphi c}$, $a_{\tau c}$) at different θ. Hence, the vector $\mathbf{a}_c$ can be explicitly expressed from (5a, b); and ϕ_1 can be derived from (3a).

The inverse harmonic model (Fig. 1d) is formulated for a 1P-OC fault remedy using a four-step procedure, and illustrated with the 5- and 6-Phase motors in Figs. 2(a, b) for clarity:

Step 1 reorganizes the operating healthy phases into N_G groups (Subsection II.A.1). To gain intuitive insights, the harmonics of $\mathbf{Q}_g$ (where g=1,…,N_G) for j=1, 3 and k=1, 3, 5, 7 are tabulated in Table I where the numbers indicates the ($|j-k|$, $|j+k|$); and the **bold** zeros correspond to j=k. For the 5- and 6-Phase examples in Figs. 2(a, b), N_G = 2 under the 1P-OC fault.

TABLE I
HARMONICS INTERACTIONS

	k=1	k=3	k=5	k=7
j=1	(**0**, 2)	(2, 4)	(4, 6)	(6, 8)
j=3	(2, 4)	(**0**, 6)	(2, 8)	(4, 10)

Step 2 determines the order number k of the current harmonics for the vector $\mathbf{i}_{gk}$ (6c), given the specified N_f. Different from the time-based inverse model, N_f and thus N_k are design parameters. To ensure the existence of the solutions to (10), the number N_k of current harmonic components should be selected such that the unknown parameters number $2N_GN_k$ in the vector $\mathbf{i}$ (6a) is larger than the dimension of the reference vector $\mathbf{q}_r$ (15a) for the ORS, and (19a) for the ERS:

$$N_k>\begin{cases}(2+3N_f)/2N_G & \text{ORS} \\ (1+2N_f)/2N_G & \text{ERS}\end{cases} \quad (21)$$

According to (21), if a large N_f for the force/torque harmonic components is considered in the inverse model, an increased N_k especially for a small N_G will result. Once N_f is selected, the smallest N_k that satisfies (21) is determined. The specific order number k can be identified from Table 1 to compensate for the corresponding force/torque harmonic components.

Assuming that (j=1) and (j=1, 3) for the examples in Figs. 2(a) and 2(b), N_f=3 and N_f=4 are chosen for the 5- and 6-Phase motors, respectively. Based on (21), $N_k \geq 3$. From Table I, the minimum N_k=3 (for k =1, 3, 5) is selected for $\mathbf{i}_{gk}$ (for g=1, 2) in (6c) to eliminate the force/torque harmonics in $\mathbf{Q}_g$ (14a) or τ_g (18a) with

$$|j \pm k| = \hbar = \begin{cases} 2, 4, 6 & \text{5-Phase motor}\left(N_f = 3\right) \\ 2, 4, 6, 8 & \text{6-Phase motor}\left(N_f = 4\right) \end{cases}$$

With $\hbar$ determined, the position-independent force/torque reference vector $\mathbf{q}_r$ formulated in (15a) for ORS and (19a) for ERS is expressed by:

$$\mathbf{q}_r = \begin{cases} \begin{bmatrix} 0 & \tau_d & \mathbf{0}_{1\times3} & \mathbf{0}_{1\times3} & \mathbf{0}_{1\times3} \end{bmatrix}^{\mathrm{T}} & \text{5-Phase motor} \\ \begin{bmatrix} \tau_d & \mathbf{0}_{1\times2} & \mathbf{0}_{1\times2} & \mathbf{0}_{1\times2} & \mathbf{0}_{1\times2} \end{bmatrix}^{\mathrm{T}} & \text{6-Phase motor} \end{cases}$$

Step 3 formulates ($\mathbf{i}_g$, $\mathbf{Z}_g$) according to (6c) and (15b) with the identified current harmonics k. Consequently, ($\mathbf{i}$, $\mathbf{Z}$) can be formulated from (6a) and (9b).

For the examples in Fig. 2,

$$\mathbf{i}_g^{\mathrm{T}} = \begin{bmatrix} \mathbf{i}_{g1}^{\mathrm{T}} & \mathbf{i}_{g3}^{\mathrm{T}} & \mathbf{i}_{g5}^{\mathrm{T}} \end{bmatrix} \tag{22}$$

With $\hbar$ (=2, 4, 6) for the 5-phase motor, the position-independent submatrix $\mathbf{Z}_g$ is derived in (23) where $\mathbf{Z}_{g(j\pm k)}$ and $\mathbf{z}_{g(k-k)}$ are defined in (14d) and (15c) respectively:

$$\mathbf{Z}_g\left(\in \mathbb{R}^{11\times6}\right) = \begin{bmatrix} \mathbf{z}_{g(1-1)} & \mathbf{0}_{3\times2} & \mathbf{0}_{3\times2} \\ \mathbf{Z}_{g(1+1)} & \mathbf{Z}_{g(1-3)} & \mathbf{0}_{3\times2} \\ \mathbf{0}_{3\times2} & \mathbf{Z}_{g(1+3)} & \mathbf{Z}_{g(1-5)} \\ \mathbf{0}_{3\times2} & \mathbf{0}_{3\times2} & \mathbf{Z}_{g(1+5)} \end{bmatrix} \tag{23}$$

Similarly, $\mathbf{Z}_g$ for the 6-phase motor with $\hbar$ (=2, 4, 6, 8) is given by (24) where $\mathbf{Z}_{g(j\pm k)}$ and $\mathbf{z}_{g(k-k)}$ are defined in (18b) and (19b) respectively:

$$\mathbf{Z}_g\left(\in \mathbb{R}^{14\times6}\right) = \begin{bmatrix} \mathbf{z}_{g(1-1)} & \mathbf{z}_{g(3-3)} & \mathbf{0}_{2\times2} \\ \mathbf{Z}_{g(1+1)} + \mathbf{Z}_{g(3-1)} & \mathbf{Z}_{g(1-3)} & \mathbf{Z}_{g(3-5)} \\ \mathbf{Z}_{g(3+1)} & \mathbf{Z}_{g(1+3)} & \mathbf{Z}_{g(1-5)} \\ \mathbf{0}_{2\times2} & \mathbf{Z}_{g(3+3)} & \mathbf{Z}_{g(1+5)} \\ \mathbf{0}_{2\times2} & \mathbf{0}_{2\times2} & \mathbf{Z}_{g(3+5)} \end{bmatrix} \tag{24}$$

With the matrix $\mathbf{Z}_g$ defined in (23) or (24), the coefficient matrix $\mathbf{Z}$ accounting all the groups can be formulated accordingly.

Step 4 solves the optimal $\mathbf{i}$ for the position-independent inverse model (10), computes the g^{th} group current $i_{g\pm}(\theta)$ from (6b) with $\mathbf{g}_{g\pm}(\theta)$ defined in (13b) for the ORS and (17b) for the ERS, and then rearranges them to accommodate with the desired $\mathbf{x}$ according to (6d).

With the derived $\mathbf{Z}$ and $\mathbf{q}_r$, $\mathbf{i}$ and $\mathbf{i}_g$ are computed off-line from (10), and the desired $\mathbf{x}$ can then be obtained in real-time as (25a) with $i_{g\pm}$ (g=1, 2) given in (25b):

$$\mathbf{x}^{\mathrm{T}} = \begin{cases} \begin{bmatrix} 0 & i_{1+} & i_{2+} & i_{2-} & i_{1-} \end{bmatrix} & \text{5-Phase motor} \\ \begin{bmatrix} 0 & i_{1+} & i_{2+} & 0 & i_{1-} & i_{2-} \end{bmatrix} & \text{6-Phase motor} \end{cases} \tag{25a}$$

where

$$i_{1(2)\pm} = \sum_{k=1,3,5} \begin{cases} \mp\mathbf{h}\left(\mp kN_P\left(\theta_{1(2)\pm} - \phi_1\right)\right)\mathbf{i}_{1(2)k} & \text{5-Phase motor} \\ -\mathbf{h}\left(-kN_P\left(\theta_{1(2)\pm} - \phi_1\right)\right)\mathbf{i}_{1(2)k} & \text{6-Phase motor} \end{cases} \tag{25b}$$

In (25b), $\theta_{1(2)\pm}=\theta-\phi_{1(2)\pm}$ and $\phi_{1(2)\pm}$ is illustrated in Fig. 2(a) for the 5-Phase motor and Fig. 2(b) for the 6-Phase motor.

III. RESULTS AND DISCUSSIONS

The inverse harmonic model (Fig. 1d) and the strategies to remedy a 1P-OC fault have been investigated numerically and experimentally; both the odd and even phase configurations characterized by different ($\mathbf{Z}$, $\mathbf{g}_{g\pm}$) formulations are considered. Specifically, the unified inverse model (10), which is applicable to remedy a 1P-OC fault of MMP-PM motors, is numerically illustrated and verified in Section III.A.1 (for a 5-phase radial-flux type motor with iron-cores) and in Section III.A.2 (for a duplex 6-phase axial-flux type ironless motor), where the remedy performances are evaluated against the conventional time-based inverse model (4). Experiments validating the inverse harmonic model and demonstrating the real-time implementation and effectiveness of the remedy algorithms on a custom-designed 6-phase motor are presented in Section III.B. As in Section II, the investigations assume Phase 1 is open-circuit.

A. Numerical Investigation of ORS and ERS

The effectiveness of the harmonic-based remedy strategy has been numerically investigated on a 5-phase and a duplex 6-phase MMP-PM motors (each with a 1P-OC fault) as shown in Table II where the parametric values used in the numerical investigations are given. In Table II, the (a_{rj}, $a_{\varphi j}$, $a_{\tau j}$) values of the 5-phase motor were computed from the magnetic flux density (MFD) fields of a finite element analysis (FEA); and that of the duplex 6-phase motor were published data in [5][26]. The 6-phase motor [5] was custom-designed to pre-eliminate any undesired forces along the Z-axis; the stator EM distribution in each phase is shown in Table II (bottom-left).

A.1 ORS for the 5-phase configuration

To provide a basis for evaluating the performance of the harmonic-based ORS, four different currents derived from the time- and harmonics-based inverse models without/with accounting for unbalanced forces are compared:

Without: TW (Time-based), HW (Harmonic-based).

With: TI (Time-based), HI (Harmonic-based).

When unbalanced forces and thus the two rows of $\mathbf{Z}_{g(j\pm k)}$ in (14d) are ignored, $\mathbf{Z}_{g(j\pm k)}$ and $\mathbf{q}_r$ in (15a,b) reduce to $a_{\tau j}\begin{bmatrix} \mp C_{\phi_\pm} & S_{\phi_\pm} \end{bmatrix}$ and $[\tau_d, 0, \ldots, 0]^{\mathrm{T}}$ respectively. Similarly, TW can be computed from (4) by replacing $\mathbf{A}$ and $\mathbf{Q}_d$ with its last row $\mathbf{a}_\tau$ and τ_d respectively. The results are summarized in Fig. 3, Fig. 4 and Table III where the copper loss ratio ζ [27] is the total copper loss in one period relative to that under healthy mode.

The following observations from the results can be made:

Parameter identification: As shown in the FEA results in Fig. 3(a), $\mathbf{a}_c$ can be characterized by its fundamental (j=1) harmonic components (a_{x1}, a_{y1}, $a_{\tau1}$) within ±1% error relative to the values computed with the FEA software. With the (a_{rj}, $a_{\varphi j}$, $a_{\tau j}$) values listed in Table II, (22), (23) and (25) are used to derive the HI and HW remedy strategies.

Under healthy mode: As compared in Figs. 3(b, c), the cogging torque τ_P is within ±0.03Nm, which is less than 0.3% of the output torque of 12Nm when the amplitude of the sinusoidal current input is maintained at 20.42A, and the corresponding unbalanced forces (f_x, f_y) are negligibly small (within ±2N) .

Under a 1P-OC fault (No remedy): As shown in Fig. 3(d), the resulting torque reduces to 9.6 Nm from that under healthy mode, and is highly oscillatory (with ±2.4Nm ripple). On the other hand, the unbalanced forces drastically increase to over 100N (with fundamental harmonic period equal to π/N_p) from less than 2N under healthy mode.

Effect of unbalanced forces in the event of a 1P-OC fault:

– *Without considering unbalanced forces*, $\mathbf{Q}_d$ reduces to a scalar τ_d. Both HW and TW remedy strategies yield almost identical (current) solutions and copper loss ratio ζ=1.29 as compared in Table III and Fig. 4(a, b). Superimposed with τ_P (Fig. 3b), an average torque (12Nm) can be maintained (Fig. 4c) but larger unbalance forces, f_x=[–120N, 120N] and f_y=[–220N, 0N], than that in Fig. 3(d) result. This is because HW (that does not account for unbalanced forces) yields larger currents than the original sinusoidal current inputs in order to sustain the healthy-mode torque. This finding suggests that the formulation can be effectively applied to a PM motor where diametrically symmetric pairs of EMs are grouped into a phase to pre-eliminate unbalanced forces.

– *With the unbalanced forces accounted in the inverse model*, HI contributes larger current amplitudes i_{gk} (k=3, 5) than those of HW (Table III) suppressing the unbalanced forces to less than ±18N while maintaining the torque at 12Nm (Fig. 4d) with copper loss ratio ζ=1.76. The residue forces may be due to the effects of the neglected **K** (2a) in the inverse model.

Validation and effectiveness of inverse harmonic model: As compared in Table III and Fig. 4(a, b), the HI (g=1, 2) group-currents are closely similar to the TI group currents. HI, characterized by three (k=1, 3, 5) harmonic components or two less than that characterized by five (k=1, 3, 5, 7, 9) harmonic components, has a slightly larger ζ than that of TI (ζ=1.65). Unlike the position-dependent TI where the harmonic components cannot be pre-determined, the number of HI harmonic components of the position independent current-vector **i** is a design parameter.

TABLE II
MAIN PARAMETRIC VALUES OF THE 5- AND 6-PHASE MOTOR

5-Phase motor

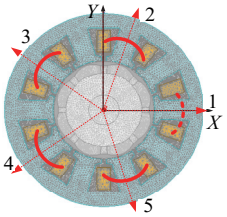

Mesh: 36,630 triangle elements

Stator EM: N_E=N_{ph} = 5, N_C =1
r_o=33.3mm, l_e=162mm
Phase 1 position:ϕ_1=0º
Rotor PM: N_P =4, r_i=31.8mm
PM arcs: ϕ_p=36.8°
thickness: l_m=7mm
Magnetizing: Radial
Computed Values:
a_{r1} = 9.55, $a_{\varphi 1}$ = −6.51,
$a_{\tau 1}$ = −0.235, K_o=0.013

6-Phase duplex motor [5][26]

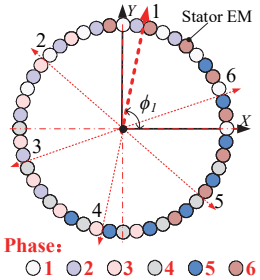

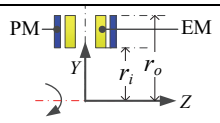

Stator EM (Single Side): N_{ph} = 6, N_E = 48, N_C =N_m =16; ϕ_1=78.75º
Rotor PM: N_P = 32, r_i=255mm, r_o=295mm, PM thickness: l_m=6mm, arcs:ϕ_p=5.625°, magnetizing: Z-axis.
Computed Value: $a_{r1}\approx a_{r3}\approx 0$;
$a_{\varphi 1}$=−6.44, $a_{\varphi 3}$=−0.36;
$a_{\tau 1}$= −1.77, $a_{\tau 3}$=−0.099.

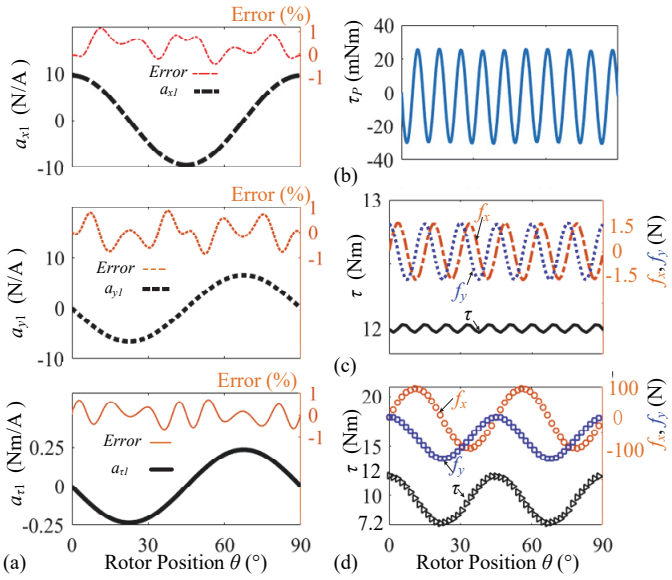

Fig. 3 5-phase motor model. (a) a_{xc}, a_{yc}, $a_{\tau c}$, (b) τ_P, (c) forces/torque under healthy mode, (d) forces/torque under 1P-OC fault.

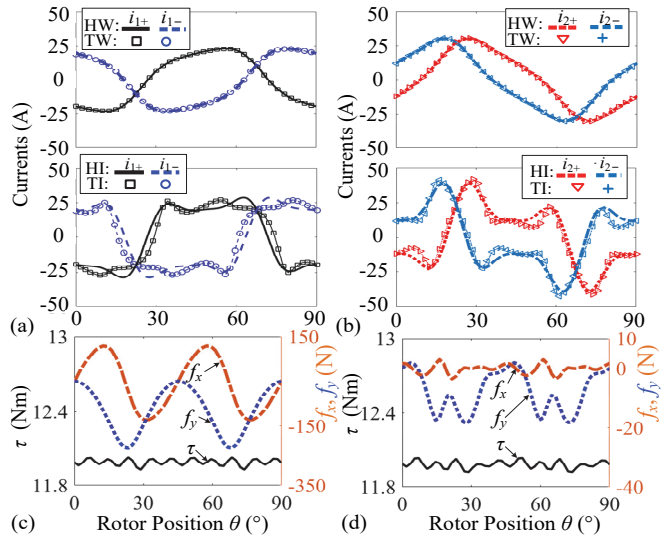

Fig. 4 5-phase motor inverse model validation: (a) Group 1 currents, (b) Group 2 currents, (c) Forces/torque with currents from HW, (d) Forces/torque with currents from HI.

TABLE III
COMPARISON OF THE 5-PHASE MOTOR INVERSE MODELS

		Group currents (i_{gk} in Amperes, α_{gk} in degrees)			
k	g	**TW**	**HW**	**TI**	**HI**
1	1	(−23.7, 4.7)	(−23.7, 4.8)	(−27.9, 7.6)	(−27.9, 2.0)
	2	(−27.6, −6.1)	(−27.6, −6.6)	(−24.1, 15.0)	(−25.3, 23.7)
3	1	(−3.0, −31.4)	(−3.0, −31.2)	(−6.5, 6.0)	(−10.6,−10.6)
	2	(3.5, −78.3)	(3.5, −78.7)	(15.2, −49.0)	(16.1,−49.7)
5	1	(−0.40,−68.2)	(−0.35,−61.6)	(−5.6, 50)	(−2.96, −18)
	2	(0.44, 33.2)	(0.48, 23.6)	(6.1, 59)	(4.78, 54)
7	1	(0, 0)	--	(1.9, −97)	--
	2	(0, 0)	--	(2.9, −13)	--
9	1	(0, 0)	--	(1.4, 33.6)	--
	2	(0, 0)	--	(−2.1, −85)	--
ζ		1.29	1.29	1.65	1.76

A.2 ERS on Six Phase Configuration

To numerically investigate the effectiveness of the inverse harmonic model (Fig. 1d) and ERS, the responses for the

following operation modes were simulated on the duplex 6-phase motor (Table II):

Mode 0 (Healthy mode or no fault operation)

Mode 1 (1P-OC fault with no remedy).

Mode 2 (Conventional method): Operated as a 3-phase motor (m = 2, 4, 6) but with phase-current double the amplitude normally operated at no-fault.

Mode 3 (Remedy with ERS): Operated as a 4-phase motor (m = 2, 3, 5, 6) with currents computed from the time-based and inverse harmonic models.

Mode 4 (Remedy with time-based model): Operated with the rest 5 phases (m = 2, 3, 4, 5, 6) with currents computed from the time-based inverse model.

The simulated currents, pulsating torque and unbalanced forces (f_x, f_y) are presented in Fig. 5. For comparison, the copper loss ratio ζ and the peak-to-peak variations of (f_x, f_y) are summarized in Table IV, where the computational times for the remedy operations in Mode 3 (inverse harmonic model) and Mode 4 (time-based inverse model) were compared in Table IV.

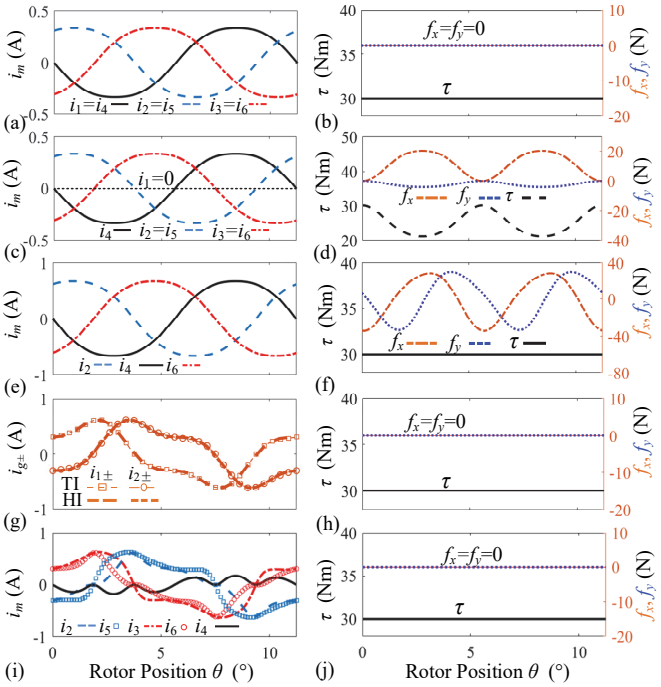

Fig. 5 6-phase motor performance under different operating modes. (a, b) Mode 0, (c, d) Mode 1, (e, f) Mode 2, (g, h) Mode 3, (i, j) Mode 4.

Some observations are drawn from the results:

Mode 0 (Fig. 5a, b): The phase-currents (m=1, 2, 3) are identical to that (m=4, 5, 6) resulting in ripple-free torque (30Nm) and zero unbalanced forces.

Mode 1 (Fig. 5c, d) leads to pulsating torque with reduced average value and unbalanced forces with a fundamental frequency at 53Hz ($2N_P$×50rpm/60).

Mode 2 (Fig. 5e, f): The torque is recovered at the cost of the unbalanced forces and doubled copper loss (ζ=2) which are the largest among all the considered operation Modes.

Mode 3 (Fig. 5g, h): The torque ripples and unbalanced forces are eliminated with reduced copper loss (ζ=1.66 in Table IV) compared with Mode 2. As a comparison, the currents were also computed using time-based inverse model; and both the time-based and harmonics-based inverse models yield nearly identical group-currents. The computational time (2μs) for the inverse harmonic model suggests that it is highly computationally efficient, and can be used for real-time control.

Mode 4 (Fig. 5i, j): Accounting for unbalanced forces, the current of Phase 4 is insignificant relative to that of non-identical diametrically symmetric phases (m=2, 3, 5, 6), since that a larger i_4 contributes to increased unbalanced forces, which have to be compensated by the currents of the other four phases. The torque ripples and unbalanced forces are eliminated, and the resulting copper loss (ζ=1.56) is only slightly smaller than that under Mode 3. The computational time for the harmonics-based method is less than 0.2% of that required by the time-based method (which involves complex matrix inversion).

TABLE IV
PEFORMANCE COMPARISON OF OPERATION MODES

Modes	**0**	**1**	**2**	**3**	**4**
ζ	1	0.83	2	1.66	1.56
f_x	0	[0, 20.2]	[−34.5, 28.0]	0	0
f_y	0	[−4.0, 0]	[−33.7, 29.6]	0	0
Computation Time (2.5GHz CPU and 16G memory):				**2μs**	**1150μs**

B. *Experimental Validation*

With the formulations of ($\mathbf{Z}$, $\mathbf{g}_{g\pm}$) numerically validated in *Subsection III.A*, the unified inverse harmonic model (Fig. 1d) accounting for MMP-PM motors with odd and even phase configurations has been experimentally validated on a duplex face-turning spindle motor [5][26] developed for machining disk-like work-pieces as shown in Fig. 6. Designed as an open platform, two sets of 48 independently controllable stator EM-windings are supplied with linear current amplifiers, which were reconfigured as a 6-phase motor in this experiment; and the winding arrangement as well as the motor parameters are illustrated in Table II. A PI-controller for the closed-loop speed control (Fig. 1c) and the current remedy algorithms were implemented on a NI Crio platform which provides an effective setup to evaluate the performances of the remedy operation.

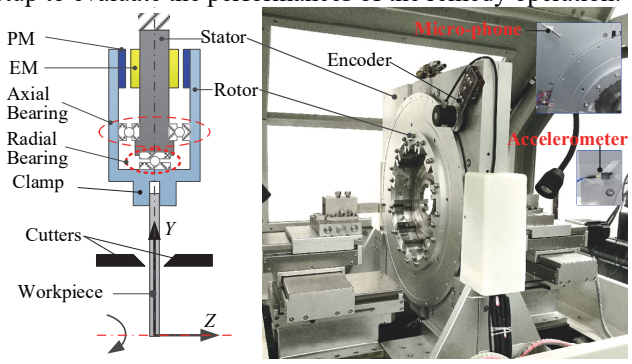

Controller: NI-CrioDriver [5]
Closed-loop linear current amplifiers (maximum ±4A each channel).

Fig. 6 Duplex PM motor [5].

A microphone (GRAS Array) installed close to the bearings (Fig. 6) on an adjustable frame was used to measure the bearing sound; and a three-axis accelerometer (PCB 356A16) was fixed on the stator surface (Fig. 6) to record the accelerations along X- and Y-axis under differ operating modes. Because of the relatively large rotational inertia (>1.9kg.m^{-2}) and PM

pole-pair number (N_P=32), the torque ripples with angular frequencies $(j\pm k)N_P$ in the experiments have little impact on the speed fluctuations and induced sound. As will be demonstrated, the measured bearing sound and vibrations due to unbalanced forces are reasonable indicators of the operation condition of the motor under 1P-OC fault.

During experiments where the motor performances under faulty and different remedy operations were compared, the motor was tested under four different operation modes (Mode 0~3 as described in *Subsection III.A.2*) at two speeds (50rpm and 85rpm) without and with cutting. To validate the effectiveness of the remedy strategies for different loading conditions, the motor was subjected to the following cutting operations of a titanium-alloy disk: 0.05mm depth-of-cutting and 0.25mm/s feed-rate at a cutting radius of 85~90mm. Experimental results are organized into four groups in Figs. 7 and 8, where the Fast Fourier Transform (FFT) of the measured sound pressures and accelerations are presented:

50rpm: Results comparing the magnitudes at the dominant frequency between without cutting (Fig. 7a) and with cutting (Fig. 7c) are given in Fig. 8(a)

85rpm: Results comparing between without cutting (Fig. 7b) and with cutting (Fig. 7d) are given in Fig. 8(b).

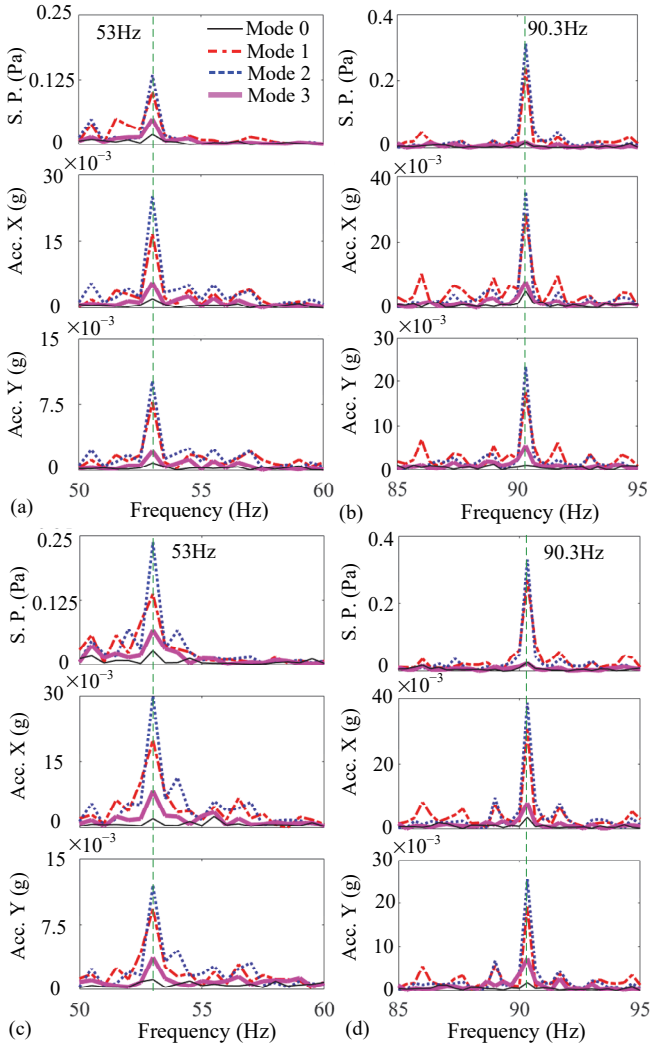

Fig. 7 FFT of bearing sound pressure and motor accelerations for four operation modes. (a) 50rpm, without cutting, (b) 85rpm, without cutting, (c) 50rpm, with cutting, (d) 85rpm, with cutting.

Some observations can be drawn based on Figs. 7 and 8:

– As shown in Fig. 7, the dominant frequencies (53Hz and 90.3Hz) correspond to the rotational speeds 50rpm and 85rpm, respectively. As compared between without and with cutting, the cutting sound (usually at a much higher frequency) has negligible effects on the bearing sound at the dominant frequencies. The apparent changes of the sound pressure and accelerations from the normal Mode 0 to faulty Mode 1 in Fig. 8 confirm that the bearing sounds and motor vibrations are reliable indicators of the motor conditions.

– As compared between Modes 0 and 1 in Fig. 8, the unbalanced forces induce large bearing sound and motor vibrations under a 1P-OC fault. The conventional remedy method (Mode 2) doubles the currents in order to maintain the spin torque, leading to aggregated unbalanced force; The (with and without cutting) comparison in Fig. 8 shows that the condition became worsen with increased loads. On the contrary, the proposed remedy method consistently reduces the unbalanced forces at different speeds and loads.

– As compared in Figs. 7 and 8, which account for all the considered operating speeds and loads of the 6-phase motor, Mode 3 and Mode 0 exhibit nearly identical sound pressure and acceleration spectrums, implying that the 1P-OC fault was remedied. The strong correlations between the numerical calculations (Fig. 5) and consistent experimental results (Figs. 7 and 8) validate the inverse harmonic model, and confirm the effectiveness and reliability of the proposed harmonic-based fault-remedy strategy for real-time implementation on a MMP-PM motor under a 1P-OC fault.

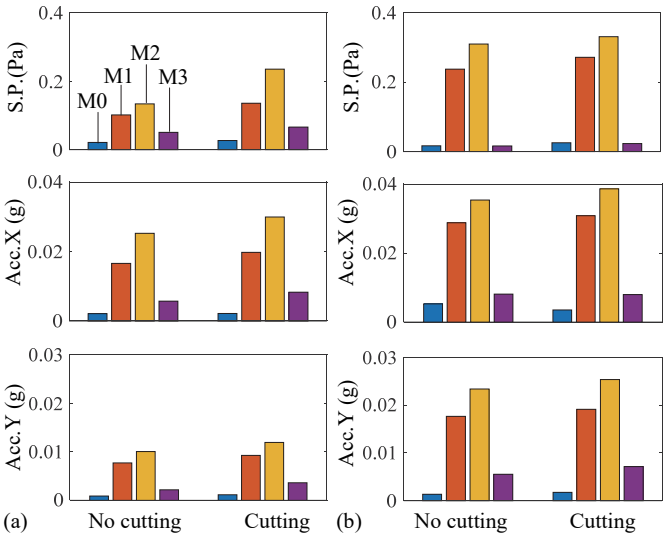

Fig. 8 Comparison of magnitudes of bearing sound pressure and accelerations of four operation modes/speeds. (a) 50rpm, (b) 85rpm.

IV. Conclusion

The method to derive a harmonic model to characterize the pulsating torque and unbalanced forces of a MMP-PM motor under an open-circuit fault and its solutions are presented. Based upon the inverse harmonic model, the remedy strategy is not only capable of recovering the motor spin torque but also effectively suppressing unbalanced forces that cause vibrations and damages on the rotor. By formulating the optimal fault-remedy currents as a combination of a position-independent

This article has been accepted for publication in a future issue of this journal, but has not been fully edited. Content may change prior to final publication. Citation information: DOI 10.1109/TMECH.2019.2906850, IEEE/ASME Transactions on Mechatronics

inverse model (can be computed offline) and a harmonic-based kernel vector, the inverse harmonic model significantly reduces the time requires to compute the remedial current (from 1150μs using a conventional time-based method to 2μs). The fault remedy methods have been numerically validated on a 5-phase and 6-phase motors, and experimentally evaluated on a custom-designed 6-phase MMP-PM motor, which demonstrate the effectiveness of the harmonic models and the remedy strategy to sustain the performance of a MMP-PM motor under a 1P-OC fault. Although illustrated with 1P-OC fault, the formulation provides physically intuitive insights into remedy operations of a MMP-PM motor under other kinds of open-circuit faults.

APPENDIX

HARMONICS-BASED FORCE/TORQUE VECTOR.

Neglecting the end-fringing effects, the force/torque vector **Q** can be derived from the Maxwell stress tensor method [22] [28]in terms of MFD $\mathbf{B}=[B_r, B_\varphi, B_z]^{\mathrm{T}}$ in cylindrical coordinates (r, φ, z) within the air-gap (enclosed between the rotor and stator):

$$\mathbf{Q}=\begin{cases}\dfrac{1}{2\mu_o}\displaystyle\int_{r_i}^{r_o} r dr \int_0^{2\pi}\begin{bmatrix}\boldsymbol{\Gamma}(\varphi)\end{bmatrix}\begin{bmatrix}0\\ -2B_z B_\varphi\end{bmatrix} d\varphi & \text{axial-flux}\\ \dfrac{l_e r_i}{2\mu_o}\displaystyle\int_0^{2\pi}\begin{bmatrix}\boldsymbol{\Gamma}(\varphi)\end{bmatrix}\begin{bmatrix}B_r^2-B_\varphi^2\\ 2B_r B_\varphi\end{bmatrix} d\varphi & \text{radial-flux}\end{cases} \tag{A.1}$$

where r_i and r_o are the inner and outer radii of the air-gap respectively, l_e is the effective length of the air-gap for radial-flux PM motor, μ_0 is the permeability of free space.

The net MFD of the PMs and c^{th} EM (denoted by the subscript 'P' and 'E_c' respectively) are expressed in harmonic forms:

$$\begin{bmatrix}B_s\\ B_\varphi\end{bmatrix}=\sum_{j=1,3,5...}^{\infty}\begin{bmatrix}B_{sPj}\cos jN_p(\varphi-\theta)\\ B_{\varphi Pj}\sin jN_p(\varphi-\theta\end{bmatrix}+\begin{bmatrix}B_{sE_c}(\varphi)\\ B_{\varphi E_c}(\varphi)\end{bmatrix} \tag{A.2}$$

where $\begin{bmatrix}B_{sEc}-B_{sE_0}\\ B_{\varphi E_c}\end{bmatrix}=\sum_{n=1,2,3...}^{\infty}\begin{bmatrix}B_{sEn}\cos n(\varphi-\beta_c)\\ B_{\varphi En}\sin n(\varphi-\beta_c)\end{bmatrix}$.

In (A.2) where $s=r$ or z, (B_{sPj} , $B_{\varphi Pj}$) are the j^{th} harmonic amplitude of (B_{sP}, $B_{\varphi P}$) that depend on the shape and magnetization of the PMs; and (B_{sEn}, $B_{\varphi En}$) is the n^{th} harmonic amplitude of (B_{sEc}, $B_{\varphi Ec}$). Using the trigonometric properties in Table A, the solutions to the integrals in the left column (where $\theta_c=\theta-\beta_c$) are given in the last column for $n=jN_P\pm1$ (otherwise, the integrals equal to zero). The integrals (A.1) can be simplified to solve for $[a_{rc}\ a_{\varphi c}\ a_{\tau c}]^{\mathrm{T}}$ in (5) for radial- and axial-flux PM motors.

The MFD terms can be derived from (A.2) leading to

$$\begin{bmatrix}B_s^2-B_\varphi^2\\ 2B_sB_\varphi\end{bmatrix}=2B_{sE0}\begin{bmatrix}B_{sP}\\ B_{\varphi P}\end{bmatrix}+ 2\sum_{n=1,2..}^{\infty}\sum_{j=1,3..}^{\infty}\begin{bmatrix}B_{sEn}B_{sPj}C_{n(\varphi-\beta_c)}C_{jN_p(\varphi-\theta)}-B_{\varphi En}B_{\varphi Pj}S_{n(\varphi-\beta_c)}S_{jN_p(\varphi-\theta)}\\ B_{sEn}B_{\varphi Pj}C_{n(\varphi-\beta_c)}S_{jN_p(\varphi-\theta)}+B_{\varphi En}B_{sPj}S_{n(\varphi-\beta_c)}C_{jN_p(\varphi-\theta)}\end{bmatrix}$$

Solving (A.1) with the above results leads to

$$\begin{bmatrix}a_{xc}\\ a_{yc}\\ a_{\tau c}\end{bmatrix}=\begin{bmatrix}\boldsymbol{\Gamma}(\beta_c) & \mathbf{0}_{2\times1}\\ \mathbf{0}_{1\times2} & 1\end{bmatrix}\sum_{j=1,3,5...}^{\infty}\begin{bmatrix}a_{rj}C_{jN_p\theta_c}\\ a_{\varphi j}S_{jN_p\theta_c}\\ a_{\tau j}S_{jN_p\theta_c}\end{bmatrix}$$

where $[a_{rj},\ a_{\varphi j}\ a_{\tau j}]^{\mathrm{T}}$ are given below for radial- and axial-flux configurations respectively with $n_{\pm}=jN_P\pm1$ and $n_0=jN_P$:

For radial flux configuration,

$$\begin{bmatrix}a_{rj}\\ a_{\varphi j}\\ a_{\tau j}\end{bmatrix}=\frac{\pi r l_e}{4\mu_0 i_m}\begin{bmatrix}\left(B_{rEn_+}-B_{\varphi En_+}\right)\left(B_{rPj}+B_{\varphi Pj}\right)+\left(B_{rEn_-}+B_{\varphi En_-}\right)\left(B_{rPj}-B_{\varphi Pj}\right)\\ -\left(B_{rEn_+}-B_{\varphi En_+}\right)\left(B_{rPj}+B_{\varphi Pj}\right)+\left(B_{rEn_-}+B_{\varphi En_-}\right)\left(B_{rPj}-B_{\varphi Pj}\right)\\ 4r_i\left(B_{\varphi En_0}B_{rPj}-B_{rEn_0}B_{\varphi Pj}\right)\end{bmatrix}$$

For axial flux configuration,

$$\begin{bmatrix}a_{rj}\\ a_{\varphi j}\\ a_{\tau j}\end{bmatrix}=\frac{\pi}{4\mu_0 i_m}\int_{r_i}^{r_o}\begin{bmatrix}r\left(B_{zEn_+}B_{\varphi Pj}+B_{\varphi En_-}B_{zPj}-B_{\varphi En_+}B_{zPj}-B_{zEn_-}B_{\varphi Pj}\right)\\ r\left(B_{\varphi En_+}B_{zPj}+B_{zEn_-}B_{\varphi Pj}-B_{zEn_+}B_{\varphi Pj}-B_{\varphi En_-}B_{zPj}\right)\\ 4r^2\left(B_{\varphi Pj}B_{zEn}-B_{\varphi En}B_{zPj}\right)\end{bmatrix}dr$$

TABLE A
ORTHOGONALITY OF TRIGONOMETRIC FUNCTIONS

Integrals	$n=jN_P\pm1$
$\int_0^{2\pi}C_{n(\varphi-\beta_c)}C_{jN_p(\varphi-\theta)}C_\varphi d\varphi=\int_0^{2\pi}S_{n(\varphi-\beta_c)}S_{jN_p(\varphi-\theta)}C_\varphi d\varphi$	$\frac{\pi}{2}C_{jN_p\theta_c\mp\beta_c}$
$\int_0^{2\pi}C_{n(\varphi-\beta_c)}S_{jN_p(\varphi-\theta)}S_\varphi d\varphi=-\int_0^{2\pi}S_{n(\varphi-\beta_c)}C_{jN_p(\varphi-\theta)}S_\varphi d\varphi$	$\mp\frac{\pi}{2}C_{jN_p\theta_c\mp\beta_c}$
$\int_0^{2\pi}C_{n(\varphi-\beta_c)}C_{jN_p(\varphi-\theta)}S_\varphi d\varphi=\int_0^{2\pi}S_{n(\varphi-\beta_c)}S_{jN_p(\varphi-\theta)}S_\varphi d\varphi$	$\mp\frac{\pi}{2}S_{jN_p\theta_c\mp\beta_c}$
$\int_0^{2\pi}C_{n(\varphi-\beta_c)}S_{jN_p(\varphi-\theta)}C_\varphi d\varphi=-\int_0^{2\pi}S_{n(\varphi-\beta_c)}C_{jN_p(\varphi-\theta)}C_\varphi d\varphi$	$-\frac{\pi}{2}S_{jN_p\theta_c\mp\beta_c}$
$\int_0^{2\pi}\left(\begin{matrix}B_{sEn}B_{\varphi Pj}C_{n(\varphi-\beta_c)}S_{jN_p(\varphi-\theta)}+\\ B_{sPj}B_{\varphi En}C_{jN_p(\varphi-\theta)}S_{n(\varphi-\beta_c)}\end{matrix}\right)d\varphi=\pi\left(\begin{matrix}B_{\varphi En}B_{sPj}-\\ B_{sEn}B_{\varphi Pj}\end{matrix}\right)S_{jN_p\theta_c}$	

REFERENCES

[1] A. Kais, J. Wang, and D. Howe. ''Torque-Ripple Minimization in Modular Permanent Magnet Brushless Machines, '' *IEEE Trans. on Ind. Appl.*, (39)6, pp. 1689-1695, 2003.

[2] M. Villani, M. Tursini, G. Fabri, and L. Castellini. "High Reliability Permanent Magnet Brushless Motor Drive for Aircraft Application," *IEEE Trans. on Ind. Elect.*, (59)5, pp. 2073-81, 2012.

[3] B. C. Mecrow, A. G. Jack, D. J. Atkinson, S. R. Green, G. J. Atkinson, A. King and B. Green. "Design and Testing of a Four-Phase Fault-Tolerant Permanent-Magnet Machine for an Engine Fuel Pump," *IEEE Trans. on Energy Conv.*, (19)4, pp. 671-8, 2004.

[4] X. Jiang, W. Huang, R. Cao, Z. Hao and W. J. "Electric Drive System of Dual-Winding Fault-tolerant Permanent-Magnet Motor for Aerospace Applications." *IEEE Trans. on Ind. Elect.*, (62)12, pp. 7322-30, 2015.

[5] K. Bai, K.-M. Lee, J. Cao, R. Xu and L. Li, ''Design and Decoupled Compensation Methods of a PM Motor Capable of 6D Force/Torque Actuation for Minimum Bearing Reaction,'' *IEEE/ASME Trans. on Mecha.,* (22)5, pp. 2252-64, 2017.

[6] K. Bai and K.-M. Lee. "Direct Field-Feedback Control of a Ball-Joint-Like Permanent-Magnet Spherical Motor," I*EEE/ASME Trans. on Mecha.,* (19)3, pp. 975-986, 2014.

[7] F. Aghili. "Energy-Efficient and Fault-Tolerant Control of Multiphase nonsinusoidal PM Synchronous Machines," *IEEE/ASME Trans. on Mecha.,* (20)6, pp. 2736-51, 2015.

[8] F. Baudart, B. Dehez, E. Matagne*, et al.*, "Torque Control Strategy of Polyphase PM Synchronous Machines with Minimal Controller Reconfiguration under Open-circuit Fault of One Phase," *IEEE Trans. on Ind. Elect.*, (59)6, pp. 2632-44, 2012.

[9] W. Sleszynski, J. Nieznanski and A. Cichowski, "Open-Transistor Fault Diagnostics in Voltage-Source Inverters by Analyzing the Load Currents," *IEEE Trans. on Ind. Elect.*, (56)11, pp. 4681-88 2009.

[10] J. Wang, A. Kais, and D. Howe. "Optimal Torque Control of Fault-Tolerant Permanent Magnet Brushless Machines." *IEEE Trans. on Magn.*, (39)5, pp. 2962-64, 2003.

[11] Z. Sun, J. Wang, G. W. Jewell and D. Howe. "Enhanced Optimal Torque Control of Fault-Tolerant PM Machine under Flux-Weakening Operation," *IEEE Trans. on Ind. Elect.*, (57)1, pp. 344-53, 2010.

[12] M. Barcaro, N. Bianchi and F. Magnussen. "Analysis and Tests of a Dual Three-phase 12-Slot 10-Pole Permanent-Magnet Motor," *IEEE Trans. on Ind. Appl.*, (46)6, pp. 23-2362, 2010.

[13] Z. Q. Zhu, M. L. Mohd Jamil and L. J. Wu. "Influence of Slot and Pole Number Combinations on Unbalanced Magnetic Force in PM Machines with Diametrically Asymmetric Windings." *IEEE Trans. on Ind. Appl.*, (49)1, pp. 19-30, 2013.

[14] L. Li, K.-M. Lee, K. Bai, X. Ouyang and H. Yang. "Inverse Models and

Harmonics Compensation for Suppressing Torque Ripples of Multiphase Permanent Magnet Motor", *IEEE Trans. on Ind. Elect.*, (65)11, pp. 8730-8739, 2018.

[15] N. Bianchi, S. Bolognani, M. D. Pré and E. Fornasiero. "Post-Fault Operations of Five-Phase Motor Using a Full-bridge Inverter," in *IEEE Power Elect. Specialists Conf.,* pp. 25-2534, Jun. 2008.

[16] N. Bianchi, S. Bolognani and M. D. Pré. "Strategies for the Fault-Tolerant Current Control of a Five-phase Permanent-Magnet Motor," *IEEE Trans. on Ind. Appl.*, (43)4, pp. 960-70, 2007.

[17] A. Mohammadpour and L. Parsa. "A Unified Fault-tolerant Current Control Approach for Five-phase PM Motors with Trapezoidal Back EMF under Different Stator Winding Connections," *IEEE Trans. on Power Elect.,* (28)7, pp. 3517-27, 2013.

[18] H. Zhou, W. Zhao, G. Liu, R. Cheng and Y. Xie. "Remedial Field-Oriented Control of Five-phase Fault-Tolerant Permanent-Magnet Motor by Using Reduced-Order Transformation Matrices.'' *IEEE Trans. on Ind. Elect.,* (64)1, pp. 169-178, 2017.

[19] L. Cheng, Y. Sui, P. Zheng, P. Wang and F. Wan. "Implem. of Post-Fault Decoupling Vector Control and Mitigation of Current Ripple for Five-Phase Fault-Tolerant PM Machine under Single-Phase Open-Circuit Fault." *IEEE Trans. on Power Elect.*, (33)10, pp. 8623-8636. 2018.

[20] G. Liu, Z. Lin, W. Zhao, Q. Chen and G. Xu. "Third Harmonic Current Injection in Fault-Tolerant Five-Phase Permanent-Magnet Motor Drive." *IEEE Trans. on Power Elect.*, (33)8, pp. 6970-6979, 2018.

[21] B. Sen and J. Wang. "Stationary frame fault-tolerant current control of polyphase PM machines under open-circuit and short-circuit faults." *IEEE Trans. on Power Elect.*, (31)7, pp. 4684-4696, 2016.

[22] L. J. Wu, Z. Q. Zhu, J. T. Chen and Z. P. Xia. "An Analytical Model of Unbalanced Magnetic Force in Fractional-slot Surface-Mounted Permanent Magnet Machines," *IEEE Trans. on Magn.*, (46)7 pp. 2686-2700, 2010.

[23] B. P. Rocandio, "*Design and Analysis of Fractional-Slot Concentrated-Winding Multiphase Fault-Tolerant Permanent Magnet Synchronous Machines*," *Ph.D. dissertation*, Sch. Eng., Univ. Navarra, Pamplona, Navarra, Spain, 2015.

[24] K.-M. Lee and H. Son. "Distributed Multipole Model for Design of Permanent-Magnet-based Actuators," *IEEE Trans. on Magn.*, (43)10, pp.3904-13, 2007.

[25] B. Hannon, P. Sergeant and L. Dupré. ''Time- and Spatial-harmonic Content in Synchronous Electrical Machines, '' *IEEE Trans. on Magn.* (53)3, pp. 1-11, 2017.

[26] K. Bai, K.-M. Lee, J. Cao and B. Hao. "Analytical Development of a Minimum Bearing Reaction Twin-Motor for Duplex Machining," in *IEEE Int. Conf. on Adv. Intell. Mecha.,* pp. 1457-62, July 2015.

[27] J. Zhu, "*Modelling, Simulation and Implementation of a Fault Tolerant Permanent Magnet AC motor Drive with Redundancy*," *Ph.D. dissertation*, School of Electrical and Electronic Eng., Univ. Adelaide, Adelaide, South Australia, Australia, 2008.

[28] K. J. Meessen, J. J. H. Paulides and E. A. Lomonova. "Force Calculations in 3-D Cylindrical Structures using Fourier Analysis and the Maxwell Stress Tensor," *IEEE Trans. on Magn*., (49)1, pp. 536-45, 2013.

Kok-Meng Lee (M'89–SM'02–F'05) received the B.S. degree in mechanical engineering from the State University of New York, Buffalo, NY, USA, in 1980, and the S.M. and Ph.D. degrees in mechanical engineering from the Massachusetts Institute of Technology, Cambridge, MA, USA, in 1982 and 1985, respectively.

He is currently Professor with the George W. Woodruff School of Mechanical Engineering, Georgia Institute of Technology, Atlanta, GA, USA. He is also Distinguished Professor with the State Key Laboratory of Digital Manufacturing Equipment and Technology, Huazhong University of Science and Technology, Wuhan, China, under the National Recruitment Program of Global Experts. His research interests include system dynamics/control, robotics, automation, and mechatronics.

Prof. Lee received the National Science Foundation Presidential Young Investigator, Sigma Xi Junior Faculty Research, International Hall of Fame New Technology, and Kayamori Best Paper Awards.

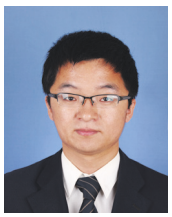

Lei Li received the B.S. degrees in mechanical engineering from Tianjin University, Tianjin, China, in 2012. He is currently working toward the Ph.D. degree with Zhejiang University, Hangzhou, China.

He was a Visiting Scholar with the George W. Woodruff School of Mechanical Engineering, Georgia Institute of Technology, Atlanta, GA, USA, during 2016-2017. His research interests include system dynamics/control and mechatronics.

Kun Bai (M'13) received the B.S. degree in control science and engineering from Zhejiang University, Hangzhou, China, in 2006, and the M.S. and Ph.D. degrees in mechanical engineering from the Woodruff School of Mechanical Engineering, Georgia Institute of Technology, Atlanta, GA, USA, in 2009 and 2012, respectively.

He is currently Associate Professor with the State Key Laboratory of Digital Manufacturing Equipment and Technology, Huazhong University of Science and Technology, Wuhan, China. His research interests include smart electromagnetic actuators/sensors and novel applications.

Xiao-ping Ouyang received the B.S. and M.S. degrees from Northeast Petroleum University, Anda, China, in 1997 and 2000, respectively, and the Ph.D. degree from Zhejiang University, Hangzhou, China, in 2005, all in mechanical engineering.

He is currently Professor with the State Key Laboratory of Fluid Power and Mechatronic Systems, Zhejiang University. His current research interests include electrohydraulic system control, aircraft hydraulics, and exoskeleton robots.

Hua-yong Yang received the B.S. degree from Huazhong University of Science and Technology, Wuhan, China, in 1982 and the Ph.D. degree from the University of Bath, Bath, U.K., in 1988.

Since 1989, he has been with Zhejiang University, Hangzhou, China, where he is the Director of the State Key Laboratory of Fluid Power and Mechatronic Systems and the Department of Mechanical Engineering. His current research interests include motion control and energy saving of mechatronic systems, fluid power components, and system development.

Prof. Yang is Academician of the Chinese Academy of Engineering. He received the first class of the National Scientific and Technological Progress Award, the National Outstanding Researcher of the Natural Science Foundation of China, and three Ministerial or Provincial Scientific and Technological Progress Prizes.